



p-Substituted Tris(2-pyridylmethyl)amines as Ligands for Highly Active ATRP Catalysts: Facile Synthesis and Characterization

Alan E. Enciso, Francesca Lorandi, Arshad Mehmood, Marco Fantin, Grzegorz Szczepaniak, Benjamin G. Janesko, and Krzysztof Matyjaszewski*

Abstract: A facile and efficient two-step synthesis of *p*-substituted tris(2-pyridylmethyl)amine (TPMA) ligands to form Cu complexes with the highest activity to date in atom transfer radical polymerization (ATRP) is presented. In the divergent synthesis, *p*-Cl substituents in tris(4-chloro-2-pyridylmethyl)amine (TPMA^{3Cl}) were replaced in one step and high yield by electron-donating cyclic amines (pyrrolidine (TPMA^{PYR}), piperidine (TPMA^{PIP}), and morpholine (TPMA^{MOR})) by nucleophilic aromatic substitution. The [Cu^{II}(TPMA^{NR₂})Br]⁺ complexes exhibited larger energy gaps between frontier molecular orbitals and >0.2 V more negative reduction potentials than [Cu^{II}(TPMA)Br]⁺, indicating >3 orders of magnitude higher ATRP activity. [Cu^I(TPMA^{PYR})]⁺ exhibited the highest reported activity for Br-capped acrylate chain ends in DMF, and moderate activity toward C–F bonds at room temperature. ATRP of *n*-butyl acrylate using only 10–25 part per million loadings of [Cu^{II}(TPMA^{NR₂})Br]⁺ exhibited excellent control.

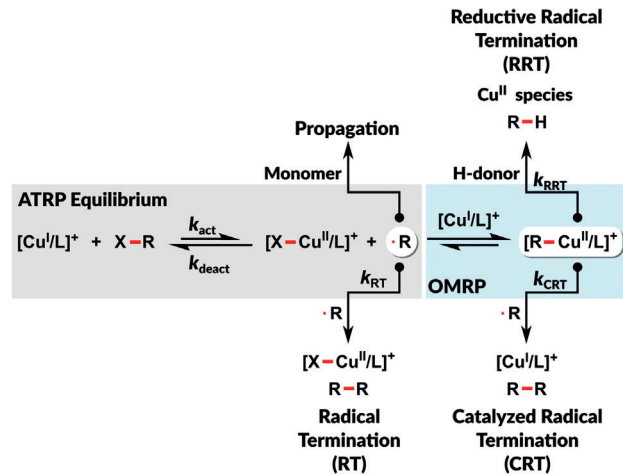
Introduction

Atom transfer radical polymerization (ATRP) is one of the most robust and widespread methods to control a radical polymerization. The versatility of ATRP has enabled the synthesis of polymers with predefined functionalities, compositions, architectures, and grafting from inorganic and biological surfaces, obtaining advanced materials for a variety of applications.^[1] Modern ATRP systems use benign reducing agents, radical initiators or external stimuli to continuously regenerate the activator form of the ATRP catalyst, such as in activators regenerated by electron transfer (ARGET) ATRP,^[2] supplemental activators and reducing agents (SARA) ATRP,^[3] initiator for continuous activator regeneration (ICAR) ATRP,^[4] photoATRP,^[5] electrochemically mediated ATRP (*e*ATRP),^[6] and mechanoATRP.^[7] These techniques have enabled to strongly decrease the catalyst

loading, finely tune polymer dispersity, achieve temporal and spatial control over polymerizations, and even complete oxygen tolerance.^[8]

The ATRP equilibrium (Scheme 1, gray region) depends on several factors: temperature, pressure, solvent, and nature of alkyl halide initiator (RX) and catalyst.^[9] The typical ATRP catalyst is a Cu complex with a multidentate N-containing ligand (L). The ATRP activator is the [Cu^I(L)]⁺ form of the complex that cleaves the C–X bond in the initiator or dormant chains, forming propagating radicals and the ATRP deactivator [Cu^{II}(L)X]⁺. The latter reacts with radicals to (re)form dormant species. This intermittent activation/deactivation process extends radicals lifetime and enables control of their propagation, thus the catalyst is largely responsible for polymerization control.

Intense efforts have been devoted to the design of catalysts with high ATRP activity, that is, high ATRP equilibrium constant K_{ATRP} .^[8a,10] The benefits of Cu/L complexes with high K_{ATRP} are numerous.^[11] First, high K_{ATRP} results in a larger fraction of [Cu^{II}(L)X]⁺ deactivator relative to [Cu^I(L)]⁺, thus enhancing the deactivation step and improving the polymerization control. Indeed, the polymer dispersity (D) decreases with increasing the concentration of [Cu^{II}(L)X]⁺.^[12] Furthermore, highly active catalysts combined with activator regeneration techniques allow for decreasing



Scheme 1. Various ATRP equilibria including radical activation/deactivation (gray region) and organometallic mediated radical polymerization (OMRP) via formation/dissociation of organometallic intermediates (blue region). Radical termination pathways include conventional, catalyzed, and reductive radical termination (RT, CRT, and RRT, respectively).

[*] Dr. A. E. Enciso, Dr. F. Lorandi, Dr. M. Fantin, Dr. G. Szczepaniak, Prof. Dr. K. Matyjaszewski

Department of Chemistry, Carnegie Mellon University
4400 Fifth Avenue, Pittsburgh, PA 15213 (USA)
E-mail: km3b@andrew.cmu.edu

A. Mehmood, Prof. Dr. B. G. Janesko
Department of Chemistry and Biochemistry
Texas Christian University
2800 South University Drive, Fort Worth, TX 76129 (USA)

Supporting information and the ORCID identification number(s) for the author(s) of this article can be found under:
<https://doi.org/10.1002/anie.202004724>.

the Cu loading to part per million (ppm) levels, while still providing good control thanks to the high fraction of deactivator. Low catalyst loadings reduce or eliminate purification steps and costs. Furthermore, high K_{ATRP} determines a low equilibrium concentration of $[Cu^I(L)]^+$ favoring temporal control over polymerizations, which come to a halt more rapidly when switching off stimuli. Finally, the small concentration of $[Cu^I(L)]^+$ activator dramatically reduces the extent of side reactions, particularly the formation of organometallic intermediates $[R-Cu^{II}(L)]^+$ (Scheme 1, blue region).^[13] This results in suppression of additional radical termination pathways caused by the reaction between $[R-Cu^{II}(L)]^+$ and propagating radicals (that is, catalyzed radical termination, CRT) or protic species (reductive radical termination, RRT).

In the ATRP of acrylates, CRT can dominate over conventional radical termination (RT) and be responsible for over 95% of termination events,^[14] thus minimizing CRT enhances the polymerization control. The formation of organometallic intermediates has been observed for both moderately and highly active ATRP catalysts.^[13a, 15] However, an increase in ATRP activity results in lower $[Cu^I(L)]^+$ and suppresses the generation of $[R-Cu^{II}(L)]^+$.^[13a] Thus, developing new catalysts with higher activity and comparable or better selectivity than existing catalysts is key to well-controlled low ppm ATRP. Optimal ATRP catalysts exhibit not only rapid activation of ATRP initiators/dormant chains but also rapid deactivation of the propagating radicals to obtain well-controlled polymerizations.^[11]

Since the discovery of ATRP in 1995, various catalysts have been developed targeting not only higher activity, but also enhanced robustness, low cost, and facile synthetic procedures.^[8a] 2,2'-Bipyridine (bpy) was the first ligand used in ATRP; then, its structure was modified by introducing different substituents in the *para* position (*p*) to the Cu-coordinating nitrogen atoms (Figure 1).^[16] Electron donating groups (EDGs) largely increased the coordination strength of ligands to Cu^{2+} and enhanced the ATRP activity of the corresponding Cu/L complexes. Tris(2-pyridylmethyl)amine (TPMA) is one of the most common ATRP ligands, particularly in aqueous media, owing to the superior stability of the Cu/TPMA complex in a broad range of pH.^[17] The ATRP activity of Cu/TPMA is about 3 orders of magnitude higher than the activity of Cu/bpy, and it was further improved by including EDGs in *p* positions on the pyridine arms of TPMA.^[16, 18]

Recently, we reported a new ATRP catalyst exhibiting 9 orders of magnitude larger activity than Cu/bpy.^[19] This highly active Cu/L complex was obtained by installing a dimethylamine group as a *p*-substituent on each pyridyl ring of TPMA, forming the tris[(4-dimethylaminopyridyl)methyl]amine ligand (TPMA^{NMe₂}, Figure 1). The high activity came at the expense of a cumbersome synthetic procedure, based on a multistep convergent path originally proposed by Karlin and co-workers (Supporting Information, Figure S1).^[20] The multistep synthesis involved hazardous conditions (gaseous dimethylamine, obtained from dimethylamine hydrochloride neutralized with sodium hydroxide, used under high pressure) and a low yield, mainly determined by the last biphasic

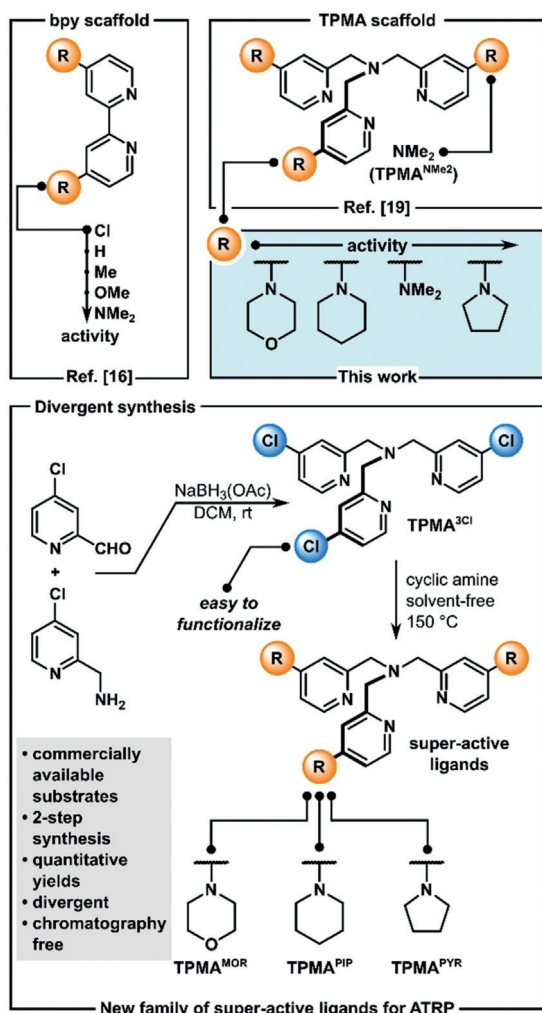


Figure 1. Divergent synthesis of *p*-substituted TPMA with cyclic amines as ligands for ATRP.

reaction step. As a consequence, the quest for a Cu-complex that simultaneously displays high ATRP activity and time- and atom-economical synthesis remains open.

Synthetic efforts in the modification of TPMA are even more desirable if one considers the widespread use of TPMA-based compounds in organic transformations. For instance, Cu/TPMA-catalyzed atom transfer radical addition (ATRA) and atom transfer radical cyclization (ATRC) enables the functionalization of unsaturated hydrocarbons.^[21] One-pot ATRA or ATRP and Cu-catalyzed azide–alkyne cycloaddition (CuAAC) has also been reported.^[22] Owing to the similar mechanism between ATRA and ATRP, highly active ATRP catalysts will also exhibit high activity in ATRA, enabling to decrease the catalyst loading, use milder conditions and expand the substrate scope.^[21a] Furthermore, complexes of TPMA with earth-abundant metals such as Cu, Fe, and Co have been used as catalysts for O_2 and CO_2 reduction reactions, and C–H oxidation.^[23] Thus, the facile synthesis of novel TPMA-based ligands with different electronic properties can give access to structure–reactivity relationships and deeper mechanistic understanding of these reactions.

Herein, we propose a green, fast, and high-yield procedure to synthesize *p*-substituted TPMA-based ligands that form Cu complexes with very high ATRP activity, comparable to or greater than the activity of Cu/TPMA^{NMe₂}. The two-step synthesis was based on a divergent approach that used commercially available precursors to afford a TPMA with *p*-Cl substituents, which was then used as a scaffold for the introduction of cyclic amines as EDGs (Figure 1). The obtained ligands, including the scaffold, and their Cu complexes were characterized and their ATRP activity and selectivity were evaluated. Finally, the complexes were used for the ATRP of *n*-butyl acrylate (BA), providing good control with catalyst loadings as low as 10 ppm.

Results and Discussion

Synthesis of *p*-Substituted TPMA-Based Compounds

The divergent synthesis of symmetrical compounds is a strategy that has shown high efficiency and scalability.^[24] This strategy was utilized to synthesize *p*-substituted TPMAs as ligands for Cu-catalyzed ATRP. The procedure comprised first the synthesis of tris-(4-chloro-2-pyridylmethyl)amine,^[25] TPMA^{3Cl}, which was then used as a scaffold by replacing the *p*-Cl groups with EDGs. TPMA^{3Cl} was obtained from commercially available precursors, via an almost quantitative reductive amination reaction between 4-chloro-2-pyridinecarbaldehyde and 4-chloro-2-pyridinemethanamine. The Cu complex with TPMA^{3Cl} is expected to exhibit relatively poor ATRP activity because of the electron-withdrawing nature of the *p*-Cl substituents. However, chlorides are versatile leaving groups that allowed for further tuning the ligand architecture.

The TPMA^{3Cl} scaffold was used to introduce different EDGs through aromatic nucleophilic substitution (S_NAr) reaction with cyclic secondary amines. By using pyrrolidine, piperidine, and morpholine, TPMA^{PYR}, TPMA^{PIP}, and TPMA^{MOR} ligands were obtained, respectively (Figure 1). As the ring size of cyclic amines decreases, the higher ring strain and the *s*-orbital character increase the orbital overlap with the electrophile, therefore enhancing the substitution rate.^[26] Using the proposed divergent synthetic route, three new ligands were prepared using a simple two-step procedure, affording high-purity compounds in gram-scale and in high yields (Table 1).

Cyclic amines are liquids, thus avoiding the difficulties in working with gaseous amines for preparing TPMA^{NMe₂}. The amount of solvents could be minimized or completely

eliminated. Some other strained amines like aziridine and azetidine were not employed in this study because their high strain could promote undesired ring-opening.^[26a,27]

Structural Studies of Cu^{II} Deactivator Complexes

The $[Cu^{II}(TPMA^{NR_2})Br]^+$ ($TPMA^{NR_2}$ collectively refers to the new ligands TPMA^{PYR}, TPMA^{PIP} and TPMA^{MOR}) complexes were crystallized following reported procedures.^[19] The determined bond lengths and angles and additional data are given in the Supporting Information, Tables S5–S7.

The geometry distortions in the complexes were analyzed using the parameters reported by Addison.^[28] The crystal structure of the $[Cu^{II}(TPMA^{MOR})Br]^+$ cation shows a trigonal bipyramidal geometry, as indicated by a structural parameter $\tau = 0.997$. Conversely, the crystal structures of the $[Cu^{II}-(TPMA^{PIP})Br]^+$ and $[Cu^{II}(TPMA^{PYR})Br]^+$ cations revealed slightly distorted trigonal bipyramidal geometries with $\tau = 0.736$ and $\tau = 0.868$. The τ value obtained for $[Cu^{II}-(TPMA^{PYR})Br]^+$ was very similar to that reported for $[Cu^{II}-(TPMA^{NMe_2})Br]^+$ ($\tau = 0.89$). It was previously observed that the Cu^{II} complex with unsubstituted TPMA, $[Cu^{II}-(TPMA)Br]^+$, exhibits a trigonal bipyramidal geometry ($\tau = 1$). Thus, the distortion from the ideal trigonal bipyramidal geometry increases in the order L = TPMA < TPMA^{MOR} < TPMA^{NMe₂} \approx TPMA^{PYR} < TPMA^{*3} (tris((4-methoxy-3,5-dimethylpyridin-2-yl)methyl)amine))^[18] < TPMA^{PIP}.^[29] Distortions from 90° in the N_{ax} –Cu– N_{eq} angles are generated by the natural bite angle of the axial ligand.^[30] The crystal structures of the new complexes showed that all Cu^{II}– N_{ax} bond distances were between 2.06 Å \leq 2.08 Å, more elongated than in $[Cu^{II}(TPMA)Br]^+$ (Cu^{II}– N_{ax} 2.040 Å),^[19,31] as well as all the Cu^{II} complexes with methyl, methoxy-substituted TPMA (Cu^{II}– N_{ax} 2.03–2.04 Å),^[29] and even $[Cu^{II}-(TPMA^{NMe_2})Br]^+$ (Cu^{II}– N_{ax} 2.047 Å).^[19] The crystal structures of all the moieties were stabilized by π – π stacking interactions between the substituted pyridine rings and by weak C–H···Br interactions (Supporting Information, Table S8 and Figure S12), as previously reported for Cu^{II} complexes with TPMA derivatives.^[19,29]

Computational Analysis

The effects of substituents on the energies of frontier molecular orbitals (MOs) of TPMA^{NR₂} were calculated. The energies of the highest-energy occupied and lowest-energy unoccupied molecular orbitals (HOMO and LUMO, respectively) and the HOMO–LUMO gap of the *p*-substituted TPMA ligands relative to the unsubstituted TPMA are shown in Table 2. The HOMO of TPMA^{PYR} had the highest relative energy, followed by TPMA^{NMe₂}, TPMA^{PIP}, and TPMA^{MOR}. A similar trend was observed for the relative energies of LUMOs, showing that these substituents destabilize TPMA, resulting in a relative decrease in the HOMO–LUMO gap. The electron-withdrawing nature of Cl contributes to lower the energies of both HOMO and LUMO via a combination of inductive and mesomeric effects by reducing the repulsive

Table 1: Yield and purity of the TPMA derivatives synthesized in this work.

Ligand	Yield [%]	Purity [%] ^[a]
TPMA ^{PYR}	Quant.	92
TPMA ^{PIP}	77	93
TPMA ^{MOR}	82	96
TPMA ^{3Cl}	Quant.	96

[a] Calculated from ¹H NMR spectra (Supporting Information, Figures S2–S8) after work-up.

Table 2: Energies of Kohn–Sham frontier molecular orbitals of *p*-substituted TPMA ligands relative to the unsubstituted TPMA calculated at M06-2X/6-311+g(d,p) level.^[a]

<i>p</i> -substituents	HOMO [eV]	LUMO [eV]	Gap [eV]
–PYR	0.862 (–6.690)	0.272 (0.168)	–0.591 (6.859)
–NMe ₂	0.678 (–6.874)	0.248 (0.144)	–0.431 (7.018)
–PIP	0.613 (–6.940)	0.224 (0.120)	–0.389 (7.060)
–MOR	0.374 (–7.178)	0.122 (0.018)	–0.253 (7.196)
–H	0 (–7.553)	0 (–0.103)	0 (7.449)
–Cl	–0.381 (–7.934)	–0.441 (–0.544)	–0.060 (7.390)

[a] The values in parentheses correspond to the effective orbital energies.

coulombic interactions between π -MOs and σ -electrons of the pyridyl moiety. The binding energies of the Cu^{II} complexes with TPMA and *p*-substituted TPMA ligands (Supporting Information, Table S5) follow the same order as the HOMO–LUMO gap values for the ligands, that is, TPMA^{PYR} > TPMA^{NMe₂} > TPMA^{PIP} > TPMA^{MOR} > TPMA > TPMA^{3Cl}.

Furthermore, the natural bond orbital analysis of unsubstituted and substituted TPMA ligands revealed that the structures of binding orbitals and hence the binding interactions are significantly controlled by stereo-electronic effects of the substituents. As shown in Figure 2a,b, the nitrogen atom in the –PYR substituent is involved in $N_{lp}–\sigma^*_C–C$ stabilizing interactions that are not present in –NMe₂. In the case of TPMA^{PIP}, the additional carbon atom in the piperidine ring led to two $N_{lp}–\sigma^*_C–H$ stabilizing interactions, further enhancing the stability of the compound (Figure 2c). In contrast, an oxygen atom in place of a –CH₂ group in the –MOR substituent resulted in a repulsive $N_{lp}–O_{lp}$ interaction (Figure 2d). Moreover, the morpholine group lacked one of the two $N_{lp}–\sigma^*_C–H$ stabilizing interactions present in –PIP, thus being less stabilized than other substituents.

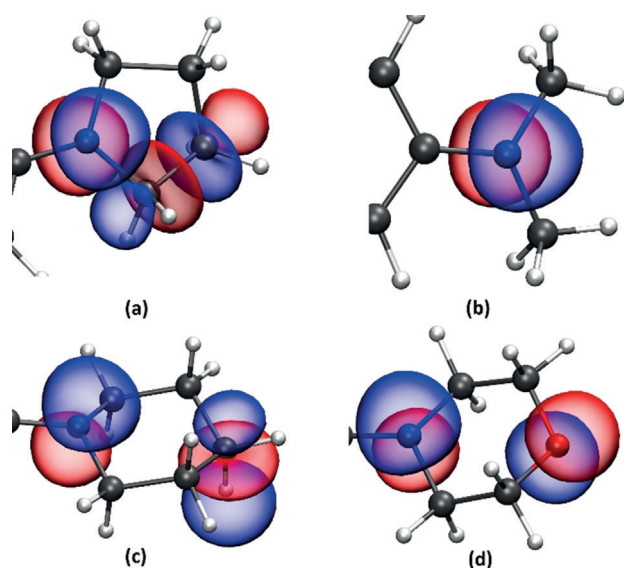


Figure 2. Close-up to natural bond orbitals of TPMA ligands substituents: a) –PYR, b) –NMe₂, c) –PIP, and d) –MOR substituents, plotted at an isovalue = 0.06 to illustrate the attractive $N_{lp}–\sigma^*_C–H$, $N_{lp}–\sigma^*_C–C$ and repulsive $N_{lp}–O_{lp}$ interactions.

DFT was then used to analyze the frontier molecular orbitals and natural charges of the complexes between Cu^{II}Br₂ and the TPMA-based ligands. The surface plots, energies, and gaps between the frontier orbitals of Cu^{II} complexes are shown in Figure 3. Additional discussion on the localization of frontier molecular orbitals is provided in the Supporting Information. The comparison of HOMO energies (E_{HOMO}) of [Cu^{II}(TPMA^{NR₂})Br]⁺ complexes and [Cu^{II}(TPMA^{3Cl})Br]⁺ relative to the E_{HOMO} of [Cu^{II}(TPMA)Br]⁺ revealed that all *p*-substituents except Cl increased E_{HOMO} owing to their electron-donating character. It was previously reported that computed E_{HOMO} values of Cu complexes with TPMA, TPMA*, and TPMA^{NMe₂} correlate to their ATRP activity, thus identifying E_{HOMO} as a good descriptor of electronic effects of the ligands on the activity of the complexes.^[32] Therefore, the increase in E_{HOMO} revealed herein suggests that the Cu complex with L = TPMA^{PYR} is the most active in ATRP, followed by the complex with L = TPMA^{PIP} and TPMA^{MOR}. The electron-withdrawing inductive and mesomeric effects of Cl substituents resulted in lower E_{HOMO} of [Cu^{II}(TPMA^{3Cl})Br]⁺ compared to the E_{HOMO} of [Cu^{II}(TPMA)Br]⁺. Analogous observations are valid for the LUMO energies of the complexes.

The calculated natural charges on Cu, Br, and axial (N_{ax}) and equatorial (N_{eq}) nitrogen atoms are listed in Table 3, together with the charges on N_{ax} and N_{eq} atoms in uncoordinated ligands for comparison. In relation to [Cu^{II}(TPMA)Br]⁺, all *p*-substituents increased the charge on N_{eq}, and the largest increase was observed for [Cu^{II}(TPMA^{PYR})Br]⁺. The charge on N_{ax} was not substantially affected by the substituents. This was attributed to the direct bonding of N_{ax} to aliphatic carbon atoms, where the effects of substitution were not transmitted as effectively as for N_{eq} atoms that were strongly affected by resonance effects. Similar trends were observed for the charges on Cu and Br atoms: the former was mostly unaffected by the ligand, while the latter was enhanced by about 0.03|e| for the NR₂ substituted ligands. The Cl substituent did not impart any significant changes in the charges on Cu and Br atoms, showing that resonance effects were more pronounced compared to inductive effects, which otherwise could cause an increase in the natural charges.

Electrochemical Analysis

The standard reduction potential (E°) of Cu/L complexes is a fundamental parameter to predict their performance as ATRP catalysts. In general, higher K_{ATRP} values correlate with more negative values of E° of [Cu^{II}(L)Br]⁺.^[8a,9b] Values of E° of binary [Cu^{II}(L)]²⁺ and ternary [Cu^{II}(L)Br]⁺ complexes with L = TPMA^{NR₂} and TPMA^{3Cl} were measured by cyclic voltammetry (CV) in DMF (Table 4). Potential values for Cu complexes with L = TPMA, TPMA*, and TPMA^{NMe₂} were in agreement with previous reports.^[19,29] The value of E° of both [Cu^{II}(L)]²⁺ and [Cu^{II}(L)Br]⁺ increased with changing the ligand in the order TPMA^{PYR} ≈ TPMA^{NMe₂} < TPMA^{PIP} < TPMA^{MOR} < TPMA* ≪ TPMA ≪ TPMA^{3Cl}. Since a circa 60 mV shift in E° of [Cu^{II}(L)Br]⁺ to more negative potentials

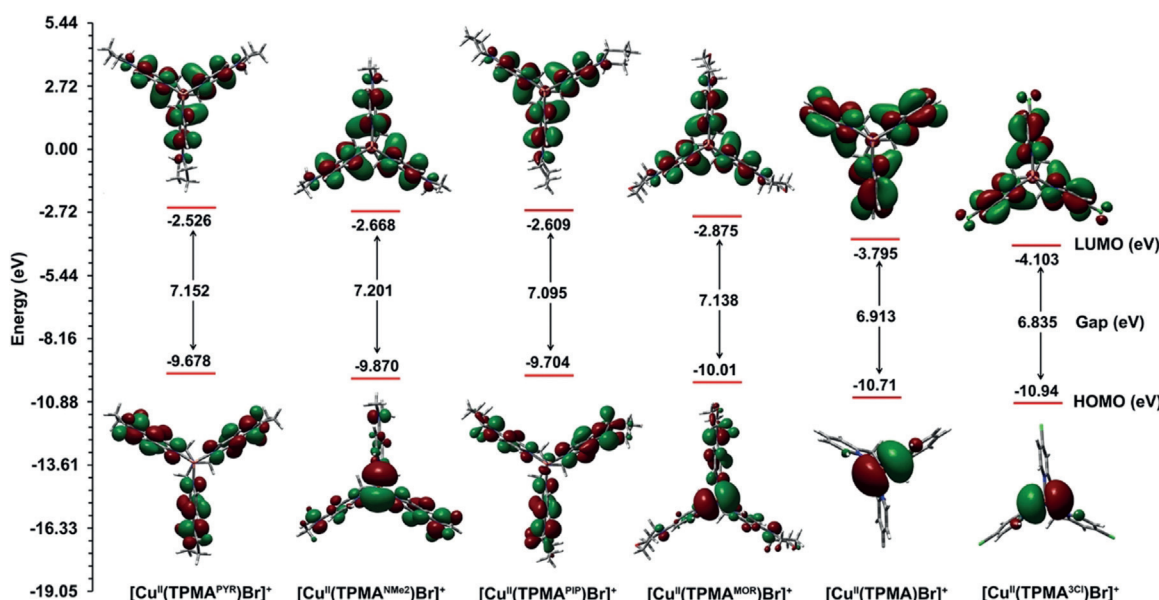


Figure 3. Kohn–Sham representation of energies and gap of the alpha HOMOs and LUMOs of Cu^{II} complexes at M06-2X/6-311+g(d,p) level (isovalue=0.02 e/bohr³).

Table 3: Calculated natural charges on selected atoms of Cu^{II} complexes with substituted and unsubstituted TPMA at M06-2X/6-311+g(d,p) level.^[a]

Complex	N _{ax}	N _{eq}	Cu	Br
[Cu ^{II} (TPMA ^{PYR})Br] ⁺	-0.593 (-0.549)	-0.602 (-0.500)	0.927	-0.554
[Cu ^{II} (TPMA ^{NMe₂})Br] ⁺	-0.584 (-0.549)	-0.598 (-0.495)	0.935	-0.549
[Cu ^{II} (TPMA ^{PIP})Br] ⁺	-0.584 (-0.548)	-0.597 (-0.486)	0.934	-0.550
[Cu ^{II} (TPMA ^{MOR})Br] ⁺	-0.594 (-0.548)	-0.594 (-0.485)	0.928	-0.546
[Cu ^{II} (TPMA)Br] ⁺	-0.587 (-0.552)	-0.548 (-0.449)	0.927	-0.528
[Cu ^{II} (TPMA ^{3Cl})Br] ⁺	-0.586 (-0.552)	-0.553 (-0.450)	0.923	-0.522

[a] The charges on nitrogen atoms for uncoordinated ligands are given in parentheses.

corresponds to an increase of one order of magnitude in K_{ATRP} ^[9b] the ATRP activity of the complexes is expected to

follow the order Cu/TPMA^{PYR} \gtrsim Cu/TPMA^{NMe₂} \gtrsim Cu/TPMA^{PIP} $>$ Cu/TPMA^{MOR} $>$ Cu/TPMA^{*3} \gg Cu/TPMA \gg Cu/TPMA^{3Cl}. The trend in E° values was in accordance with Cu^I/Cu^{II} oxidation energies computed by DFT in the gas phase (Supporting Information, Figure S16). The oxidation energies of binary Cu complexes relative to [Cu^I(TPMA)]⁺/[Cu^{II}(TPMA)]²⁺ increased with E° shifting to more negative values. Only the complex with L=TPMA^{3Cl} exhibited more positive oxidation energies relative to the complex with L=TPMA.

CV of binary [Cu^{II}(L)]²⁺ and ternary [Cu^{II}(L)Br]⁺ complexes with L=TPMA^{NR₂} and TPMA^{3Cl} was also conducted in CH₃CN (E ; Supporting Information, Table S12). The order of E° values was similar to the one observed in DMF, except for TPMA^{NMe₂} \lesssim TPMA^{PYR}. Thus, the trend in ATRP activity of the catalysts should be similar in both solvents, with Cu/TPMA^{PYR}, Cu/TPMA^{NMe₂} and Cu/TPMA^{PIP} exhibiting the highest activity. It is worth noting that Cu/TPMA^{PYR} is expected to exhibit 4 and 9 orders of magnitude higher K_{ATRP} than Cu/TPMA and Cu/bpy, respectively, thus displaying similar activity to Cu/TPMA^{NMe₂}, while being accessible

Table 4: Thermodynamic parameters for Cu complexes with unsubstituted and *p*-substituted TPMA, in DMF at $T=25^\circ\text{C}$.

Ligand	$E^\circ_{[\text{Cu}^{II}(L)]^{2+}/[\text{Cu}^I(L)]^+}$ (V vs. SCE)	$E^\circ_{[\text{BrCu}^{II}(L)]^+/\text{BrCu}^I(L)}$ (V vs. SCE)	β^{II}/β^{I} ^[a]	$k_{\text{disp}} [\text{M}^{-1} \text{s}^{-1}]$ ^[b]	$K_{\text{Br}}^I [\text{M}^{-1}]$ ^[c]	$K_{\text{Br}}^{II} [\text{M}^{-1}]$ ^[d]	σ_p ^[e]	N ^[f]
TPMA ^{PYR}	-0.385	-0.503	2.1×10^6	6.6	1.1×10^3	1.1×10^5	-0.89 ^[g]	15.9
TPMA ^{NMe₂}	-0.365	-0.497	9.7×10^5	3.5×10^1	7.0×10^2	1.2×10^5 ^[h]	-0.83	15.8
TPMA ^{PIP}	-0.353	-0.484	6.1×10^5	7.8	6.7×10^2	1.1×10^5	-0.63 ^[g]	-
TPMA ^{MOR}	-0.316	-0.433	1.4×10^5	2.0×10^1	1.1×10^3	1.0×10^5	-0.55 ^[g]	14.6
TPMA ^{*3} ^[h]	-0.269	-0.385	6.6×10^4	7.7	1.3×10^4	4.2×10^5	-0.41	-
TPMA ^[h]	-0.141	-0.232	1.6×10^2	1.7	1.2×10^4	4.2×10^5	0	12.9
TPMA ^{3Cl}	-0.097	-0.122	2.8×10^1	1.5	6.4×10^5	1.7×10^6	0.23	11.7

[a] Calculated from Equation (1), by using $E^\circ_{\text{Cu}^{2+}/\text{Cu}^+} = -0.011$ V vs. SCE. [b] Measured by rotating disk electrode (see the Supporting Information, Experimental Procedures). [c] Calculated from Equation (2). [d] Measured by UV/Vis-NIR titrations (Supporting Information, Figure S1). [e] From Ref. [34], unless otherwise specified. [f] From Ref. [35]. [g] Obtained in this work by DFT calculations, as described in the Supporting Information. [h] From Ref. [13a], except for the k_{disp} values for L=TPMA and TPMA^{*3} that were measured in this work.

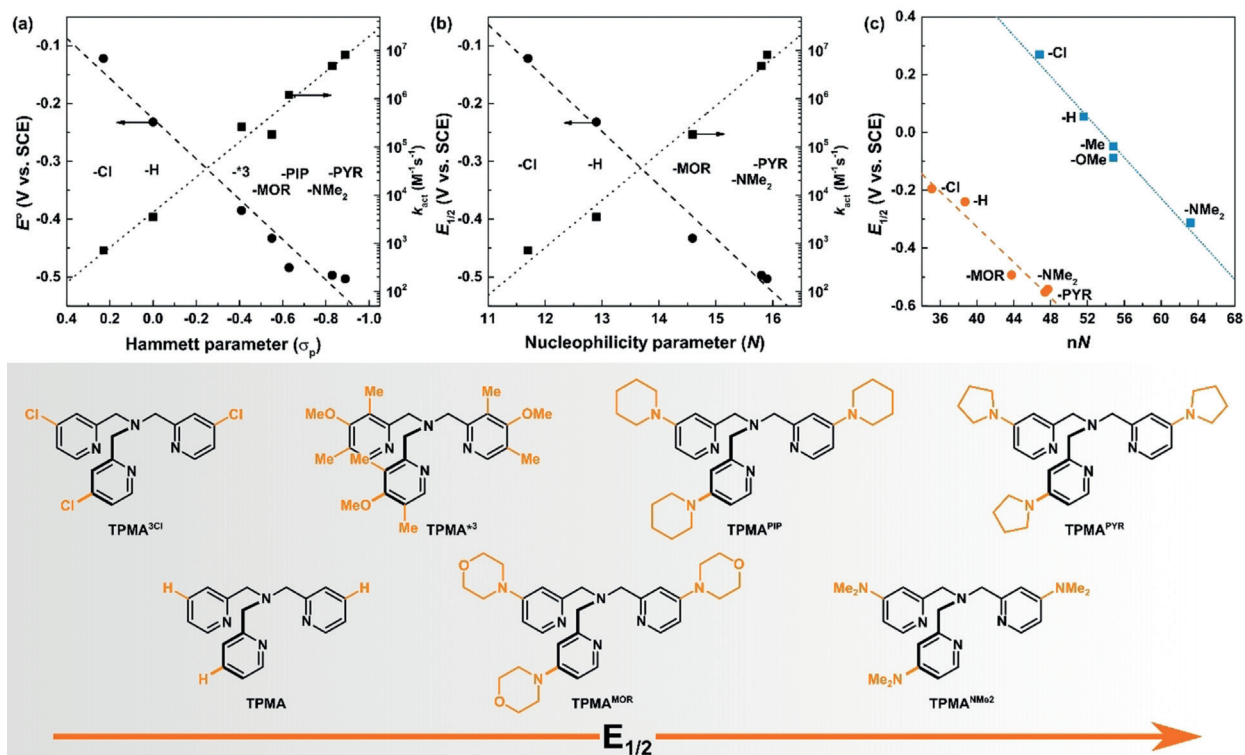


Figure 4. a,b) Plot of E° of $[\text{Cu}^{\text{II}}(\text{L})\text{Br}]^+$ (measured in DMF, dots) and k_{act} of $[\text{Cu}^{\text{I}}(\text{L})]^+$ (measured in DMF for $\text{RX} = \text{MBP}$, squares) as a function of σ_p (a) and N (b) of the substituents in *para* position on the pyridine rings of TPMA. c) Comparison between the variation of E° of $[\text{Cu}^{\text{II}}(\text{L})\text{Br}]^+$ (measured in MeCN) with N of the substituents multiplied by the number of *p*-substituents (n) for Cu complex, with $\text{L} = p$ -substituted bpy (blue squares) and *p*-substituted TPMA (orange dots) and $n = 4$ for the bpy family ($\text{Cu}/2\text{bpy}$), and $n = 3$ for the TPMA family.

through a much more sustainable synthetic procedure than Cu/TPMA^{NMe₂}.^[33]

The E° of the catalysts shifted to more negative values with increasing the electron-donating character of the *p*-substituents. Indeed, a linear relationship was observed between E° values of $[\text{Cu}^{\text{II}}(\text{L})\text{Br}]^+$ and the Hammett parameter (σ_p) of the substituents (Table 4 and Figure 4a).^[34] The values of σ_p of -MOR, -PIP, and -PYR were determined via DFT calculations, as described in the Supporting Information. Since K_{ATRP} increases with E° of $[\text{Cu}^{\text{II}}(\text{L})\text{Br}]^+$ becoming more negative, K_{ATRP} (that is, the catalyst activity) is predicted to increase with decreasing σ_p . Moreover, the effect of *p*-substituents on pyridine rings can be evaluated through the nucleophilicity parameter N (Table 4),^[35] which was observed to linearly scale with E° of $[\text{Cu}^{\text{II}}(\text{L})\text{Br}]^+$ (Figure 4b). Indeed, a linear relationship was previously reported between N of *p*-substituted pyridines and σ_p of the substituents (Supporting Information, Figure S18).^[35] The E° values of Cu complexes with *p*-substituted bpy were previously shown to shift to more negative values with decreasing σ_p of the substituents (Supporting Information, Figure S20).^[16] Herein, we observed a similar trend in E° values of $[\text{Cu}^{\text{II}}(\text{L})\text{Br}]^+$ ($\text{L} = p$ -substituted bpy) with increasing N of the substituents. Interestingly, when the number of *p*-substituents for Cu complex (n) was considered, almost identical slopes were obtained in the linear regressions of E° values vs. $n\sigma_p$ for both TPMA and bpy families (Supporting Information, Figure S20b). The same behavior was found for E° values vs. nN of both L families

(Figure 4c). Thus, σ_p and N values can be used to predict the ATRP activity of different families of ATRP catalysts. Given the abundance of σ_p and N values reported in the literature, the correlations identified in this work can guide the design of new ATRP catalysts.

The E° values of binary Cu complexes allows the determination of the ratio between the stability constants of $[\text{Cu}^{\text{II}}(\text{L})]^{2+}$ and $[\text{Cu}^{\text{I}}(\text{L})]^+$, that is, $\beta^{\text{II}}/\beta^{\text{I}}$, calculated by using Equation (1):

$$E_{\text{Cu}^{2+}/\text{Cu}^+}^\circ - E_{[\text{Cu}^{\text{II}}(\text{L})]^{2+}/[\text{Cu}^{\text{I}}(\text{L})]^+}^\circ = \frac{RT}{F} \ln \frac{\beta^{\text{II}}}{\beta^{\text{I}}} \quad (1)$$

where $E_{\text{Cu}^{2+}/\text{Cu}^+}^\circ$ is the reduction potential of the solvated Cu salt, with no added ligand, R is the gas constant, F is Faraday's constant, and T is the temperature. The $\beta^{\text{II}}/\beta^{\text{I}}$ ratio for the Cu/TPMA^{NR₂} complexes were 3–5 orders of magnitude higher than for Cu/TPMA, in both DMF and CH₃CN, indicating that *p*-substituted TPMA ligands with EDGs enhanced the stabilization of Cu^{II} compared to TPMA. Conversely, the electron-withdrawing nature of Cl led to a lower $\beta^{\text{II}}/\beta^{\text{I}}$ ratio for Cu/TPMA^{3Cl} compared to Cu/TPMA. All binary complexes exhibited a quasi-reversible voltammetric response, indicating that $[\text{Cu}^{\text{I}}(\text{L})]^+$ species were stable in the CV timescale. However, $[\text{Cu}^{\text{I}}(\text{L})]^+$ species tends to disproportionate to give metallic Cu and $[\text{Cu}^{\text{II}}(\text{L})]^{2+}$, particularly in solvents with high polarity. This disproportionation reaction consumes the ATRP activator $[\text{Cu}^{\text{I}}(\text{L})]^+$ and thus it can be

detrimental in polymerization. The equilibrium constant of disproportionation K_{disp} is typically proportional to the kinetic constant of disproportionation k_{disp} .^[17] The latter was determined for all Cu^I complexes with unsubstituted and substituted TPMA in DMF (Table 4; Supporting Information, Figure S21). Similar k_{disp} values were obtained for L = TPMA*, TPMA^{PIP}, and TPMA^{PYR}, whereas Cu complexes with L = TPMA^{MOR} and TPMA^{NMe₂} exhibited 2–3 times faster disproportionation, indicating that Cu/TPMA^{PIP} and Cu/TPMA^{PYR} can be a better choice for ATRP in solvents that promote rapid disproportionation, such as water.^[17]

Finally, the difference between E° values of binary and ternary complexes provided the ratio between the halidophilicity (that is, halide affinity) constants of [Cu^{II}(L)]²⁺ and [Cu^I(L)]⁺, that is, $K_{\text{Br}}^{\text{II}}/K_{\text{Br}}^{\text{I}}$, according to Equation (2):

$$E^\circ_{[\text{Cu}^{\text{II}}(\text{L})]^{2+}/[\text{Cu}^{\text{I}}(\text{L})]^{+}} - E^\circ_{[\text{Cu}^{\text{II}}(\text{L})\text{Br}]^{+}/[\text{Cu}^{\text{I}}(\text{L})\text{Br}]} = \frac{RT}{F} \ln \frac{K_{\text{Br}}^{\text{II}}}{K_{\text{Br}}^{\text{I}}} \quad (2)$$

Activation of Alkyl Halides by [Cu^I(L)]⁺

The ability of the novel Cu complexes to activate alkyl bromide (RBr) initiators was probed by electrochemical techniques. In particular, CV combined with simulations (see details in the Supporting Information) needed to be used for the highly active Cu/TPMA^{NR₂} catalysts, while a rotating disk electrode (RDE) could be used for the far less active Cu/TPMA^{Cl}. In DMF, RBr = methyl 2-bromopropionate (MBP), which mimics the acrylate chain ends (Table 5, Figure 5; Supporting Information, Figure S24).^[13a] In CH₃CN, ethyl α-bromoisobutyrate (EBiB) was used as initiator (Supporting Information, Figures S23, S25) for comparison with data in the previous report.^[9a] In both systems, RBr activation by Cu/TPMA^{MOR}, Cu/TPMA^{PIP}, Cu/TPMA^{PYR}, as well as by the previously reported Cu/TPMA^{NMe₂} showed the total catalysis phenomenon (Supporting Information, Figure S22), which is typically observed for a catalytic process occurring with very high rate constant ($>10^6 \text{ M}^{-1} \text{ s}^{-1}$).^[19]

As expected, k_{act} values increased with $E^\circ_{[\text{Cu}^{\text{II}}(\text{L})\text{Br}]^{+}/[\text{Cu}^{\text{I}}(\text{L})\text{Br}]}$ shifting to more negative values.^[9a] In DMF, $E^\circ_{[\text{Cu}^{\text{II}}(\text{L})\text{Br}]^{+}/[\text{Cu}^{\text{I}}(\text{L})\text{Br}]}$ for L = TPMA^{PYR} was slightly more negative than for L = TPMA^{NMe₂} and this resulted in almost twice higher activity of Cu/TPMA^{PYR} compared to Cu/TPMA^{NMe₂}, which was previously reported as the most active ATRP catalyst.^[19] The activity of Cu/TPMA^{Cl} in DMF was four times lower than the activity of Cu/TPMA, as expected from the electron-withdrawing nature of Cl.

The logarithm of k_{act} values was found to scale linearly with both Hammett and nucleophilicity parameters if the substituents (Figure 4a,b). This relationship can be explained considering that 1) a linear relation exists between E° of [Cu^{II}(L)Br]⁺, thus its K_{ATRP} and the values of σ_p and N of the substituents; and 2) changes in K_{ATRP} are primarily dictated by the ability of the catalyst to activate the initiator/dormant chains, whereas the deactivation reaction is less affected by the catalyst nature.^[11]

In CH₃CN with EBiB, the activity of Cu/TPMA^{PIP}, Cu/TPMA^{NMe₂}, and Cu/TPMA^{PYR} was very similar ($k_{\text{act}} = 1.5\text{--}2 \times 10^7 \text{ M}^{-1} \text{ s}^{-1}$). Overall, the simple two-step divergent synthetic approach proposed herein effectively yielded novel ATRP catalysts with comparable or even higher activity to the most active known ATRP catalyst.

Furthermore, the high activity of Cu/TPMA^{PYR} was confirmed by measuring the activation of an alkyl fluoride. Fluoroalkanes are typically non accessible by ATRP, owing to the very high strength of C–F bonds.^[9a] However, [Cu^I(TPMA^{PYR})]⁺ successfully activated diethyl fluoromalonate (DEFM) in DMF at room temperature, with a moderate value of $k_{\text{act}} = 5.2 \text{ M}^{-1} \text{ s}^{-1}$ (Supporting Information, Figure S26). This value is three orders of magnitude higher than for [Cu^I(TPMA)]⁺ under similar conditions^[36] and it is comparable to the activation of acrylate mimic initiators by seminal bpy-based ATRP catalysts.

Formation and Stability of Organometallic Intermediates

Moderately and highly active Cu^I ATRP activators can react not only with initiators or halogen-capped chain ends, but also with propagating radicals, forming organometallic intermediates [R–Cu^{II}(L)]⁺, similar to the organometallic mediated radical polymerization (OMRP, Scheme 1).^[13a,37] As a consequence, propagating radicals in ATRP can be deactivated by reacting with either [Cu^{II}(L)X]⁺ (ATRP deactivation with rate constant k_{deact}), or with [Cu^I(L)]⁺ (OMRP deactivation, $k_{\text{d,OMRP}}$). The [R–Cu^{II}(L)]⁺ intermediate can 1) dissociate back to R· and [Cu^I(L)]⁺ (OMRP activation, $k_{\text{a,OMRP}}$); 2) react with a propagating radical to form dead chains and regenerate [Cu^I(L)]⁺ (CRT, k_{CRT}); or 3) react with proton donors in solution (such as impurities, excess ligand) forming a saturated chain and a Cu^{II} species that is inactive in ATRP (RRT, k_{RRT}).^[13b,38]

The interplay between the ATRP and OMRP equilibria for a catalyst/initiator system was evaluated by CV followed

Table 5: Ligand effect on the formation of organometallic species from Cu^{II}Br₂/L and MBP in DMF.

	TPMA ^{PYR}	TPMA ^{NMe₂} ^[a]	TPMA ^{PIP}	TPMA ^{MOR}	TPMA ^{*3} ^[a]	TPMA ^[a]
$k_{\text{act}} [\text{M}^{-1} \text{ s}^{-1}]$	8.1×10^6	4.8×10^6	1.2×10^6	1.8×10^5	2.6×10^5	3.5×10^3
$k_{\text{deact}} [\text{M}^{-1} \text{ s}^{-1}]$	5.1×10^7	1.6×10^7	6.0×10^7	4.0×10^6	4.0×10^7	1.8×10^8
K_{ATRP}	1.6×10^{-1}	3.1×10^{-1}	2.0×10^{-2}	4.5×10^{-2}	6.5×10^{-3}	1.9×10^{-5}
$k_{\text{a,OMRP}} [\text{s}^{-1}]$	30	2.3	0.4	2	0.8	3.4×10^2
$k_{\text{d,OMRP}} [\text{M}^{-1} \text{ s}^{-1}]$	5×10^8	2.0×10^8	6×10^7	3×10^7	8.0×10^7	1.3×10^9
$K_{\text{OMRP}} [\text{M}]$ ^[b]	6×10^{-8}	1.2×10^{-8}	7×10^{-9}	7×10^{-8}	1.0×10^{-8}	2.6×10^{-7}
$k_{\text{CRT}} [\text{M}^{-1} \text{ s}^{-1}]$	4×10^6	8×10^5	8×10^6	2×10^6	3×10^5	9×10^6

[a] From Ref. [13a]. [b] $K_{\text{OMRP}} = k_{\text{a,OMRP}}/k_{\text{d,OMRP}}$.

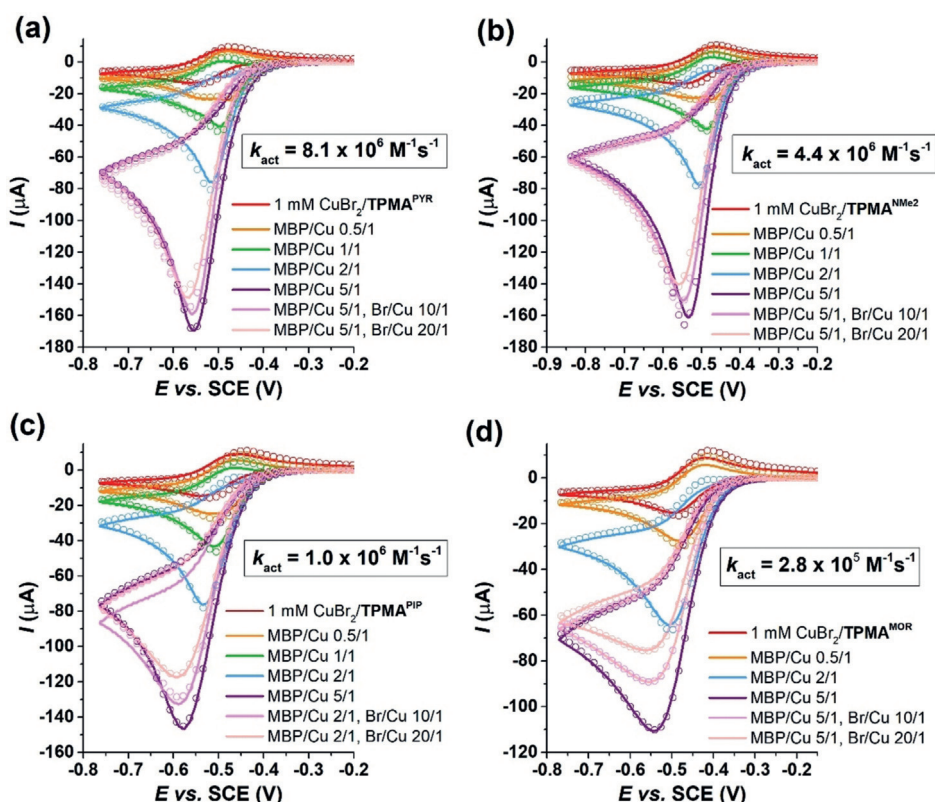


Figure 5. Experimental (solid lines) and simulated (dots) CVs for the activation of MBP in DMF by $[Cu^1(L)]^+$, with L = a) TPMA^{PYR}, b) TPMA^{NMe₂}, c) TPMA^{PIP}, and d) TPMA^{MOR}. Recorded on a GC disk at a scan rate of 0.2 V/s, in DMF + 0.1 M Et₄NBF₄ + 0.05 M TEMPO, 1 mM CuBr₂/L, and increasing amounts of MBP and Et₄NBr.

by simulations,^[15,39] and further validated by spectroscopic investigation and PREDICI simulation^[40] of the reaction between $[Cu^1(L)]^+$ and an initiator.^[13a] Herein, MBP was used as acrylate-mimic initiator, and experiments were conducted in anhydrous DMF, with a stoichiometric amount of L to Cu, to minimize the contribution of RRT. Results are shown in the Supporting Information, Figures S27–S29, and summarized in Table 5 and the Supporting Information, Table S14, together with previously reported data for L = TPMA, TPMA*, and TPMA^{NMe₂}.^[13a]

The value of k_{deact} was reported to slightly decrease with increasing the activity of the catalyst.^[9a,13a] Indeed, all of the catalysts analyzed in this work exhibited lower k_{deact} than Cu/TPMA.

However, k_{deact} values for Cu/TPMA^{PIP} and Cu/TPMA^{PYR} were 1.3–3.8 times higher than for Cu/TPMA*³ and Cu/TPMA^{NMe₂}, suggesting that these new catalysts could promote faster radical deactivation, thus enhancing polymerization control, particularly under conditions where Cu-catalyzed side reactions are minimized (for example, low Cu loading, methacrylates and styrene ATRPs).^[13a]

For each catalyst, the rate constant of organometallic formation was $k_{d,OMRP} \approx 10^8 M^{-1}s^{-1}$, in agreement with previous analyses.^[13a,15,39] The value of $k_{a,OMRP}$ was generally low, indicating slow dissociation of $[R-Cu^{II}(L)]^+$, which accelerated in the order L = TPMA^{PIP} ≈ TPMA*³ < TPMA^{NMe₂} ≈ TPMA^{MOR} < TPMA^{PYR} < TPMA. The rate constant of CRT was generally relatively high (10^5 – $10^6 M^{-1}s^{-1}$) and increased in the order L = TPMA*³ < TPMA^{NMe₂} < TPMA^{MOR} <

TPMA^{PYR} < TPMA^{PIP} ≈ TPMA. This analysis further supports our previous observations that no precise correlation exists between ATRP catalyst activity and selectivity, and that the ligand nature affects much more the ATRP equilibrium than the OMRP equilibrium.^[13a]

Moreover, under polymerization conditions, the equilibrium concentration of $[Cu^1(L)]^+$ decreases with increasing the activity of the catalyst. Therefore, by using the most active catalysts reported herein, the fraction of total Cu in the $[Cu^1(L)]^+$ form is < 1% in typical ATRP systems,^[13a] thus minimizing the impact of CRT and/or RRT on the polymerization control.

ATRP with Low ppm Catalyst Loadings

The ability of Cu/TPMA^{PYR}, Cu/TPMA^{PIP}, and Cu/TPMA^{MOR} to control the ATRP of *n*-butyl acrylate (BA) using very low catalyst loadings (10 to 25 molar ppm relative to BA) was investigated, by performing ICAR ATRP with AIBN (2,2'-azobis(2-methylpropionitrile)) as conventional radical initiator and EBiB as ATRP initiator (Supporting Information, Table S15). The performance of the Cu complex with the TPMA^{3Cl} scaffold was also tested.

ICAR ATRP catalyzed by 10 ppm of Cu/TPMA^{NR2} displayed linear semilogarithmic kinetic plots (Supporting Information, Figure S30), reaching 70–80% monomer conversion within 4 h. Obtained polymers had molecular weight (MW) matching the theoretical value (Figure 6), however the

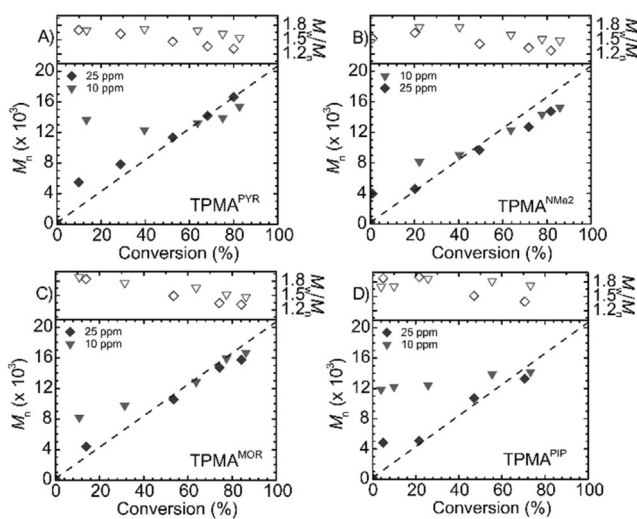


Figure 6. Evolution of PBA molecular weight (bottom of each graph) and dispersity (top) with conversion. General conditions of ICAR ATRP of BA: [BA]₀/[EBiB]₀/[CuBr₂L]₀/[AIBN]₀ = 160:1:0.016–0.0016:0.2, T = 60 °C, [BA]₀ = 4.5 M, in anisole. L = a) TPMA^{PYR}, b) TPMA^{NMe₂}, c) TPMA^{MOR}, and d) TPMA^{PIP}.

dispersity D was close to 1.5 or slightly higher, owing to the relatively low amount of $[\text{Cu}^{II}(\text{TPMA}^{\text{NR}2})\text{Br}]^+$ deactivator. Indeed, by increasing the catalyst loading to 25 ppm, the polymerization rates remained similar, and MW values matched with theoretical values, while polymer dispersity decreased to $D \approx 1.3$.

In contrast, higher loading of $[\text{Cu}^{II}(\text{TPMA}^{\text{3Cl}})\text{Br}]^+$ was needed to obtain a controlled polymerization, due to the low K_{ATRP} for this catalyst. The ICAR ATRP of BA with 50 ppm of $[\text{Cu}^{II}(\text{TPMA}^{\text{3Cl}})\text{Br}]^+$ was poorly controlled, giving a polymer with $D \approx 3$ (Supporting Information, Table S15).

The polymerization control improved by increasing the catalyst loading to 100 ppm. BA conversion of 90% was reached after 13 h, yielding polymer with pre-determined MW and $D \approx 1.5$.

These experiments confirmed the importance of using electron-donating substituents on the TPMA scaffold to provide good control with low ppm catalyst loadings. Although the novel highly active catalysts form organometallic intermediates with acrylate radicals, the contribution of this side reaction and consequent terminations (that is, CRT and RRT) is less important under polymerization conditions. Indeed, the high K_{ATRP} of the catalysts ensured that only a very small fraction was present as $[\text{Cu}^I(\text{L})]^+$ during polymerizations. Furthermore, OMRP and CRT parameters are less affected by the solvent than ATRP parameters,^[13a] suggesting that even better control can be achieved in more polar solvents.

Conclusion

p-Substituted TPMA-based ligands for Cu catalyzed ATRP were synthesized through a facile two-step procedure in very high yield. The new ligands formed Cu complexes with

very high ATRP activity, similar or even higher than the currently most active ATRP catalyst, Cu/TPMA^{NMe₂}. The synthesis was based on a divergent approach and represents a significant improvement in terms of atom-economy, chemical hazard and cost compared to the reported procedure for the synthesis of TPMA^{NMe₂}.

The novel TPMA-based ligands with cyclic amines as *p*-substituents and their Cu complexes were characterized by X-ray, UV/Vis-NIR spectroscopy and cyclic voltammetry. DFT calculations provided values of HOMO-LUMO gaps, binding energies, and relative $[\text{Cu}^{II}(\text{L})]^{2+}/[\text{Cu}^I(\text{L})]^+$ oxidation energies that complemented the experimental results and confirmed the ATRP activity order of the complexes. In particular, Cu/TPMA^{PYR} was the most ATRP active among the new compounds, displaying activity similar or higher than Cu/TPMA^{NMe₂}. These highly active catalysts were closely followed by Cu/TPMA^{PIP} and then Cu/TPMA^{MOR}. Thus, the size of the cyclic amines affected the electron-donating properties of the *p*-substituted TPMA ligands, in turn modifying the activity of the resulting ATRP catalysts. On the other hand, TPMA^{3Cl}, which was used as scaffold to produce the other ligands, was less active than the Cu complex with unsubstituted TPMA, due to the electron-withdrawing nature of Cl.

The Cu complex with TPMA^{PYR} exhibited moderate room-temperature activity toward a poorly reactive alkyl fluoride initiator. The complexes with TPMA^{NR₂} ligands provided well-controlled ATRPs with only 25 or even 10 ppm of catalyst. The high values of K_{ATRP} of these catalysts resulted in a very small equilibrium concentration of $[\text{Cu}^I(\text{L})]^+$ during polymerization, while the vast majority of the catalyst was present in the $[\text{Cu}^{II}(\text{L})\text{Br}]^+$ deactivator form. As a consequence, 1) the catalyst loading could be decreased without losing polymerization control, and 2) side reactions promoted by $[\text{Cu}^I(\text{L})]^+$, such as the formation of organometallic species and CRT, were suppressed. These active catalysts can be potentially used for ATRP of less activated monomers or for atom transfer radical addition reactions with less active alkyl halides. Moreover, these catalysts could provide enhanced temporal control in ATRP, owing to the low equilibrium concentration of Cu^I/L activator. The extension of the library of ATRP catalysts and the deeper understanding of their activity, selectivity, and stability demonstrated in this work can increase the monomer and initiator scope of ATRP.

Acknowledgements

The financial support from NSF (CHE 1707490 and CHE 2000391) is gratefully acknowledged. A.E.E. acknowledges the Mexican Council for Science and Technology—CONACyT for the postdoctoral award (291231-2do año de Continuidad de Estancias Posdoctorales en el Extranjero Vinculadas a la Consolidación de Grupos de Investigación) and Sir J. Fraser Stoddart for permitting him to complete this manuscript. G.S. acknowledges the Polish Ministry of Science and Higher Education (“Mobilnosc Plus” grant no. 1646/MOB/V/2017/0) for financial support.

Conflict of interest

The authors declare no conflict of interest.

Keywords: amine ligands · ATRP · catalysis · copper · polymer synthesis

- [1] a) K. Matyjaszewski, *Macromolecules* **2012**, *45*, 4015–4039; b) K. Matyjaszewski, *Adv. Mater.* **2018**, *30*, 1706441; c) M. Kamigaito, T. Ando, M. Sawamoto, *Chem. Rev.* **2001**, *101*, 3689–3746.
- [2] K. Matyjaszewski, W. Jakubowski, K. Min, W. Tang, J. Huang, W. A. Braunecker, N. V. Tsarevsky, *Proc. Natl. Acad. Sci. USA* **2006**, *103*, 15309.
- [3] a) P. Krys, Y. Wang, K. Matyjaszewski, S. Harrisson, *Macromolecules* **2016**, *49*, 2977–2984; b) A. Anastasaki, V. Nikolaou, G. Nurumbetov, P. Wilson, K. Kempe, J. F. Quinn, T. P. Davis, M. R. Whittaker, D. M. Haddleton, *Chem. Rev.* **2016**, *116*, 835–877; c) D. Konkolewicz, Y. Wang, P. Krys, M. Zhong, A. A. Isse, A. Gennaro, K. Matyjaszewski, *Polym. Chem.* **2014**, *5*, 4396–4417; d) D. Konkolewicz, Y. Wang, M. Zhong, P. Krys, A. A. Isse, A. Gennaro, K. Matyjaszewski, *Macromolecules* **2013**, *46*, 8749–8772; e) C. M. R. Abreu, P. V. Mendonça, A. C. Serra, A. V. Popov, K. Matyjaszewski, T. Guliashvili, J. F. J. Coelho, *ACS Macro Lett.* **2012**, *1*, 1308–1311; f) J. P. Mendes, P. V. Mendonça, P. Maximiano, C. M. R. Abreu, T. Guliashvili, A. C. Serra, J. F. J. Coelho, *RSC Adv.* **2016**, *6*, 9598–9603.
- [4] D. Konkolewicz, A. J. Magenau, S. E. Averick, A. Simakova, H. He, K. Matyjaszewski, *Macromolecules* **2012**, *45*, 4461–4468.
- [5] a) M. Chen, M. Zhong, J. A. Johnson, *Chem. Rev.* **2016**, *116*, 10167–10211; b) L. Fu, Z. Wang, S. Lathwal, A. E. Enciso, A. Simakova, S. R. Das, A. J. Russell, K. Matyjaszewski, *ACS Macro Lett.* **2018**, *7*, 1248–1253; c) X. Pan, M. A. Tasdelen, J. Laun, T. Junkers, Y. Yagci, K. Matyjaszewski, *Prog. Polym. Sci.* **2016**, *62*, 73–125.
- [6] P. Chmielarz, M. Fantin, S. Park, A. A. Isse, A. Gennaro, A. J. D. Magenau, A. Sobkowiak, K. Matyjaszewski, *Prog. Polym. Sci.* **2017**, *69*, 47–78.
- [7] a) H. Mohapatra, M. Kleiman, A. P. Esser-Kahn, *Nat. Chem.* **2017**, *9*, 135; b) Z. Wang, Z. Wang, X. Pan, L. Fu, S. Lathwal, M. Olszewski, J. Yan, A. E. Enciso, Z. Wang, H. Xia, K. Matyjaszewski, *ACS Macro Lett.* **2018**, *7*, 275–280.
- [8] a) T. G. Ribelli, F. Lorandi, M. Fantin, K. Matyjaszewski, *Macromol. Rapid Commun.* **2019**, *40*, 1800616; b) S. Dadashi-Silab, K. Matyjaszewski, *Macromolecules* **2018**, *51*, 4250–4258; c) J. Yeow, R. Chapman, A. J. Gormley, C. Boyer, *Chem. Soc. Rev.* **2018**, *47*, 4357; d) A. E. Enciso, L. Fu, A. J. Russell, K. Matyjaszewski, *Angew. Chem. Int. Ed.* **2018**, *57*, 933–936; *Angew. Chem.* **2018**, *130*, 945–948; e) A. E. Enciso, L. Fu, S. Lathwal, M. Olszewski, Z. Wang, S. R. Das, A. J. Russell, K. Matyjaszewski, *Angew. Chem. Int. Ed.* **2018**, *57*, 16157–16161; *Angew. Chem.* **2018**, *130*, 16389–16393; f) M. Rolland, R. Whitfield, D. Messmer, K. Parkatzidis, N. P. Truong, A. Anastasaki, *ACS Macro Lett.* **2019**, *8*, 1546–1551; g) X. Pan, M. Fantin, F. Yuan, K. Matyjaszewski, *Chem. Soc. Rev.* **2018**, *47*, 5457–5490; h) F. A. Leibfarth, K. M. Mattson, B. P. Fors, H. A. Collins, C. J. Hawker, *Angew. Chem. Int. Ed.* **2013**, *52*, 199–210; *Angew. Chem.* **2013**, *125*, 210–222; i) Z. Wang, J. Yan, T. Liu, Q. Wei, S. Li, M. Olszewski, J. Wu, J. Sobieski, M. Fantin, M. R. Bockstaller, K. Matyjaszewski, *ACS Macro Lett.* **2019**, *8*, 859–864; j) R. Whitfield, N. P. Truong, D. Messmer, K. Parkatzidis, M. Rolland, A. Anastasaki, *Chem. Sci.* **2019**, *10*, 8724–8734; k) R. Whitfield, K. Parkatzidis, M. Rolland, N. P. Truong, A. Anastasaki, *Angew. Chem. Int. Ed.* **2019**, *58*, 13323–13328; *Angew. Chem.* **2019**, *131*, 13457–13462.
- [9] a) W. Tang, Y. Kwak, W. Braunecker, N. V. Tsarevsky, M. L. Coote, K. Matyjaszewski, *J. Am. Chem. Soc.* **2008**, *130*, 10702–10713; b) W. A. Braunecker, N. V. Tsarevsky, A. Gennaro, K. Matyjaszewski, *Macromolecules* **2009**, *42*, 6348–6360.
- [10] V. Doan, B. B. Noble, A. K. K. Fung, M. L. Coote, *J. Org. Chem.* **2019**, *84*, 15624–15632.
- [11] F. Lorandi, K. Matyjaszewski, *Isr. J. Chem.* **2020**, *60*, 108–123.
- [12] a) E. Mastan, S. Zhu, *Macromolecules* **2015**, *48*, 6440–6449; b) P. Krys, K. Matyjaszewski, *Eur. Polym. J.* **2017**, *89*, 482–523.
- [13] a) M. Fantin, F. Lorandi, T. G. Ribelli, G. Szczepaniak, A. E. Enciso, C. Fliedel, L. Thevenin, A. A. Isse, R. Poli, K. Matyjaszewski, *Macromolecules* **2019**, *52*, 4079–4090; b) L. Thevenin, C. Fliedel, K. Matyjaszewski, R. Poli, *Eur. J. Inorg. Chem.* **2019**, 4489–4499.
- [14] M. R. Martinez, J. Sobieski, F. Lorandi, M. Fantin, S. Dadashi-Silab, G. Xie, M. Olszewski, X. Pan, T. G. Ribelli, K. Matyjaszewski, *Macromolecules* **2020**, *53*, 59–67.
- [15] T. J. Zerk, L. R. Gahan, E. H. Krenske, P. V. Bernhardt, *Polym. Chem.* **2019**, *10*, 1460–1470.
- [16] A. J. D. Magenau, Y. Kwak, K. Schröder, K. Matyjaszewski, *ACS Macro Lett.* **2012**, *1*, 508–512.
- [17] M. Fantin, A. A. Isse, A. Gennaro, K. Matyjaszewski, *Macromolecules* **2015**, *48*, 6862–6875.
- [18] K. Schröder, R. T. Mathers, J. Buback, D. Konkolewicz, A. J. Magenau, K. Matyjaszewski, *ACS Macro Lett.* **2012**, *1*, 1037–1040.
- [19] T. G. Ribelli, M. Fantin, J.-C. Daran, K. F. Augustine, R. Poli, K. Matyjaszewski, *J. Am. Chem. Soc.* **2018**, *140*, 1525–1534.
- [20] a) C. X. Zhang, S. Kaderli, M. Costas, E.-i. Kim, Y.-M. Neuhold, K. D. Karlin, A. D. Zuberbühler, *Inorg. Chem.* **2003**, *42*, 1807–1824; b) B. Lucchese, K. J. Humphreys, D.-H. Lee, C. D. Incarvito, R. D. Sommer, A. L. Rheingold, K. D. Karlin, *Inorg. Chem.* **2004**, *43*, 5987–5998.
- [21] a) T. Pintauer, K. Matyjaszewski, *Chem. Soc. Rev.* **2008**, *37*, 1087–1097; b) A. J. Clark, *Eur. J. Org. Chem.* **2016**, 2231–2243.
- [22] a) C. L. Ricardo, T. Pintauer, *Eur. J. Inorg. Chem.* **2011**, 1292–1301; b) J. Geng, J. Lindqvist, G. Mantovani, D. M. Haddleton, *Angew. Chem. Int. Ed.* **2008**, *47*, 4180–4183; *Angew. Chem.* **2008**, *120*, 4248–4251.
- [23] a) S. Fukuzumi, Y. M. Lee, W. Nam, *ChemCatChem* **2018**, *10*, 9–28; b) D. He, T. Jin, W. Li, S. Pantovich, D. Wang, G. Li, *Chem. Eur. J.* **2016**, *22*, 13064–13067; c) B. Mühlendorf, R. Wolf, *Angew. Chem. Int. Ed.* **2016**, *55*, 427–430; *Angew. Chem.* **2016**, *128*, 437–441; d) S. L.-F. Chan, T. L. Lam, C. Yang, J. Lai, B. Cao, Z. Zhou, Q. Zhu, *Polyhedron* **2017**, *125*, 156–163; e) M. Langerman, D. G. Hetterscheid, *Angew. Chem. Int. Ed.* **2019**, *58*, 12974–12978; *Angew. Chem.* **2019**, *131*, 13108–13112.
- [24] a) A. E. Enciso, F. Ramirez-Crescencio, M. Zeiser, R. Redón, E. E. Simanek, *Polym. Chem.* **2015**, *6*, 5219–5224; b) J. Shimokawa, *Tetrahedron Lett.* **2014**, *55*, 6156–6162; c) S. Raut, A. E. Enciso, G. M. Pavan, C. Lee, A. Yepremyan, D. A. Tomalia, E. E. Simanek, Z. Gryczynski, *J. Phys. Chem. C* **2017**, *121*, 6946–6954.
- [25] A. Beni, A. Dei, S. Laschi, M. Rizzitano, L. Sorace, *Chem. Eur. J.* **2008**, *14*, 1804–1813.
- [26] a) E. E. Simanek, H. Abdou, S. Lalwani, J. Lim, M. Mintzer, V. J. Venditto, B. Vittur, *Proc. R. Soc. London Ser. A* **2010**, *466*, 1445–1468; b) L. R. Caswell, M. E. Goldsmith, *J. Org. Chem.* **1989**, *54*, 5101–5104.
- [27] a) S. Patra, B. Kozura, A. Y. T. Huang, A. E. Enciso, X. Sun, J.-T. Hsieh, C.-L. Kao, H.-T. Chen, E. E. Simanek, *Org. Lett.* **2013**, *15*, 3808–3811; b) K. X. Moreno, E. E. Simanek, *Tetrahedron Lett.* **2008**, *49*, 1152–1154.
- [28] A. W. Addison, T. N. Rao, J. Reedijk, J. van Rijn, G. C. Verschoor, *J. Chem. Soc. Dalton Trans.* **1984**, 1349–1356.
- [29] A. Kaur, T. G. Ribelli, K. Schröder, K. Matyjaszewski, T. Pintauer, *Inorg. Chem.* **2015**, *54*, 1474–1486.

- [30] H. C. Fry, H. R. Lucas, A. A. Narducci Sarjeant, K. D. Karlin, G. J. Meyer, *Inorg. Chem.* **2008**, *47*, 241–256.
- [31] T. J. Zerk, P. V. Bernhardt, *Coord. Chem. Rev.* **2018**, *375*, 173–190.
- [32] C. Fang, M. Fantin, X. Pan, K. de Fiebre, M. L. Coote, K. Matyjaszewski, P. Liu, *J. Am. Chem. Soc.* **2019**, *141*, 7486–7497.
- [33] J. Qiu, K. Matyjaszewski, L. Thouin, C. Amatore, *Macromol. Chem. Phys.* **2000**, *201*, 1625–1631.
- [34] C. Hansch, A. Leo, R. Taft, *Chem. Rev.* **1991**, *91*, 165–195.
- [35] F. Brotzel, B. Kempf, T. Singer, H. Zipse, H. Mayr, *Chem. Eur. J.* **2007**, *13*, 336–345.
- [36] S. Lanzalaco, M. Fantin, O. Scialdone, A. Galia, A. A. Isse, A. Gennaro, K. Matyjaszewski, *Macromolecules* **2017**, *50*, 192–202.
- [37] a) Y. Wang, N. Soerensen, M. Zhong, H. Schroeder, M. Buback, K. Matyjaszewski, *Macromolecules* **2013**, *46*, 683–691; b) T. G. Ribelli, S. M. Wahidur Rahaman, J.-C. Daran, P. Krys, K. Matyjaszewski, R. Poli, *Macromolecules* **2016**, *49*, 7749–7757.
- [38] L. Thevenin, C. Fliedel, M. Fantin, T. G. Ribelli, K. Matyjaszewski, R. Poli, *Inorg. Chem.* **2019**, *58*, 6445–6457.
- [39] T. J. Zerk, P. V. Bernhardt, *Inorg. Chem.* **2017**, *56*, 5784–5792.
- [40] M. Wulkow, *Macromol. React. Eng.* **2008**, *2*, 461–494.

Manuscript received: March 31, 2020

Revised manuscript received: May 10, 2020

Accepted manuscript online: May 16, 2020

Version of record online: June 17, 2020